remote sensing

MDPI

Article

Remote Sensing of Soil Alkalinity and Salinity in the Wuyu'er-Shuangyang River Basin, Northeast China

Lin Bai [1,2], Cuizhen Wang [1,3], Shuying Zang [1,*], Yuhong Zhang [1], Qiannan Hao [1] and Yuexiang Wu [4]

1 Key Laboratory of Remote Sensing Monitoring of Geographic Environment, College of Heilongjiang Province, Harbin Normal University, Harbin, Heilongjiang 150025, China; bail986@163.com (L.B.); CWANG@mailbox.sc.edu (C.W.); zhangyuhong77@163.com (Y.Z.); hqn558@163.com (Q.H.)

2 Department of Human Geography and Urban-Rural Planning, Qiqihar University, Qiqihar, Heilongjiang 161006, China

3 Department of Geography, University of South Carolina, Columbia, SC 29208, USA

4 Qiqihar Meteorological Bureau, Qiqihar, Heilongjiang 161006, China; qxjwyx@163.com

* Correspondence: zsy6311@163.com; Tel.: +86-451-8806-0689

Academic Editors: José A.M. Demattê, Magaly Koch and Prasad S. Thenkabail
Received: 2 December 2015; Accepted: 29 January 2016; Published: 20 February 2016

Abstract: The Songnen Plain of the Northeast China is one of the three largest soda saline-alkali regions worldwide. To better understand soil alkalinization and salinization in this important agricultural region, it is vital to explore the distribution and variation of soil alkalinity and salinity in space and time. This study examined soil properties and identified the variables to extract soil alkalinity and salinity via physico-chemical, statistical, spectral, and image analysis. The physico-chemical and statistical results suggested that alkaline soils, coming from the main solute Na_2CO_3 and $NaHCO_3$ in parent rocks, characterized the study area. The pH and electric conductivity (EC) were correlated with both narrow band and broad band reflectance. For soil pH, the sensitive bands were in short wavelength (VIS) and the band with the highest correlation was 475 nm (r = 0.84). For soil EC, the sensitive bands were also in VIS and the band with the highest correlation was 354 nm (r = 0.84). With the stepwise regression, it was found that the pH was sensitive to reflectance of OLI band 2 and band 6, while the EC was only sensitive to band 1. The R^2_{Adj} (0.73 and 0.72) and root mean square error (RMSE) (0.98 and 1.07 dS/m) indicated that, the two stepwise regression models could estimate soil alkalinity and salinity with a considerable accuracy. Spatial distributions of soil alkalinity and salinity were mapped from the OLI image with the RMSE of 1.01 and 0.64 dS/m, respectively. Soil alkalinity was related to salinity but most soils in the study area were non-saline soils. The area of alkaline soils was 44.46% of the basin. Highly alkaline soils were close to the Zhalong wetland and downstream of rivers, which could become a severe concern for crop productivity in this area.

Keywords: soil alkalinity; soil salinity; spectral signature; Landsat 8 OLI; Songnen Plain

1. Introduction

Soil alkalinization and salinization is the process of accumulation of free salts such as Na^+, K^+, Ca^{2+}, Mg^{2+}, and Cl^- in subsoil and groundwater, which leads to soil degradation and hinders the growth of plants [1,2]. When Na^+ is the main source of salinization, it is also called sodification that is usually associated with increasing pH of soil. Development of salinity, alkalinity, and sodicity in soils decreases productivity in croplands and limits the diversity of grass species in pastureland [3].

The Songnen Plain in the Northeast China is one of the three largest soda saline-alkali regions in the world [4]. The saline-alkali soils in this region can be explained by soil parent material, terrain, and climate. Firstly, the plain is surrounded by the Changbai, Xiaoxing'an, and Daxing'an Mountain Ranges where alkali rocks contain abundant sodium aluminosilicates such as orthoclase, plagioclase, albite, sodalite, and nepheline [5]. These alkali rocks serve as parent materials of soil and are closely related to soil alkalinization and salinization in this region. Secondly, the neotectonic movement shaped the plain's geomorphic pattern that favors soil salinizing and alkalizing [5]. Surrounded by mountains on three sides, the plain has poor drainage characterized with closed flows, ephemeral rivers, and wetlands on flat landscapes. Drainage is often blocked and salt could not leach out [6]. Most salt-affected areas are related to the lacustrine depressions, especially where temporary waterlogging occurs because of insufficient natural drainage [1]. Thirdly, the plain has a typical continental monsoon climate with annual air temperature varying from −18 °C to 23 °C and annual precipitation from 300 mm to 600 mm [7]. The average annual evaporation is 1200–1800 mm that is 2–3.5 times higher than annual precipitation [8]. Soluble saline compounds are thus accumulated in soils, resulting in soil salinization and alkalinization. Within this climate, the freeze-thawing process is closely related to soil alkalinization in the plain [9]. During the freezing stage, water in the bottom soil moves up and salt is accumulated in the frozen layers. In thawing stage, salt in the frozen layer is transported to the topsoil by strong evaporation. In this process, the frozen layers block the soil-water exchange between soil surface and groundwater [10]. Additionally, human-related factors such as intensified agricultural management for crop and livestock production also play important roles in soil alkalinization and salinization. Soil alkalinization and salinization, especially in grasslands, are one of the most severe environmental threats to the cold, fragile, eco-systems of the Songnen Plain. Currently, salt-affected land accounts for about 18.8% of the plain and newly salinized/alkalized land has been observed every year [1,4].

Alkalinization and salinization are primary causes of soil degradation and productivity reduction. Being involved in complex physical and chemical interactions, these processes could occur within a time period as short as one decade and are generally irreversible [11]. Therefore, it is vital to explore the processes and variety of alkalinity and salinity in both spatial and temporal dimensions. Past studies have been conducted to quantify soil alkalinity and salinity via physico-chemical analysis. In such a measure of soil acidity or alkalinity [12,13], the pH is an important indicator of soil healthiness. Plants can take up nutrients from soil only when pH is in a moderate range (6.0–7.5). In highly alkaline soils, iron, manganese, and phosphorus are less available [14]. It is commonly accepted that soil with pH above 7.5 is considered alkaline [15,16]. Alkalinization, the increase of soil pH, is also associated with sodification [1]. The exchangeable sodium percentage (ESP) is an indicator of sodic /non-sodic characteristics. Soil salinity is often measured by EC of the soil/water suspension that estimates the total amount of dissolved ions in water [17]. According to Rhoades [18], an EC threshold of 4 dS/m defines the boundary between saline and non-saline soils.

Remote sensing is an efficient tool to expand the physico-chemical analysis to large spatial scales in a span of decades. For example, Dwivedi [19] applied the Landsat MSS data to examine the temporal changes of salt-affected soils in the Indo-Gangetic alluvial plain. With principal component analysis, the study extracted soil brightness and vegetation greenness from spectral reflectance to examine the changes in the extent of salt-affected soils. In Shamsi *et al.* [20], the moderate resolution imaging spectroradiometer (MODIS) images were used to produce soil salinity maps. The MODIS imagery, assisted with soil sampling data, was also used to measure soil salinity in the Red River Valley [21]. Visual interpretation of false color composite (FCC) could detect different levels of soil alkalinity and salinity [22,23]. However, analytical interpretation relied on human experiences, which made the results subjective and less comparable in different seasons. Digital image processing techniques were also applied to detect soil salinity/ alkalinity using multi-spectral imagery. In Metternicht and Zinck [24], six TM bands were used to classify salt- and sodium-affected soil types. Metternicht [25] applied the fuzzy logic to detect salt types based on anion ratios from a Landsat

TM image in a salt-affected area of Bolivia. Different classifiers were evaluated in Dwivedi and Sreenivas [26] to test the accuracies of mapping salt-affected soils in the Indo-Gangetic alluvial plains. A stepwise regression procedure was performed to extract the relationship between MODIS bands, ratios, principal components (PCs), and soil property variables [20]. These image-based efforts, however, are strongly affected by sensor resolutions, seasons of image acquisition, study areas, and the applied methods [27,28].

Limited by the broad band spectral properties, classification accuracies were commonly low in these studies. Attempts have been made to study soil salinity and alkalinity with field spectra and hyper-spectral imagery. Curve configurations of spectral signatures extracted from hyper-spectral imagery could be the most important clues to characterize soil salinity and alkalinity [29]. Exploring spectral data in the partial least-squares regression model (PLSR), Wang *et al.* [30] found that the reflectance in visible (VIS) bands (400–750 nm) was more sensitive to soil pH than other spectral regions. Ong and Cudahy [31] estimated soil pH using lab spectra and airborne hyperspectral sensor (Hymap) image. A soil salinity spectral index was constructed at 2052 nm and 2203 nm to estimate soil salt content from a Hyperion image to map soil salinity [32]. Liu *et al.* [33] used soil spectral index derived from continuum removal to predict pH values and evaluate the salinity degrees of soda saline-alkali soil in the west of Jilin province, China. The availability of hyper-spectral imagery, however, is limited, which makes the above-mentioned approaches less applicable.

Recent attempts began to combine spectra and multi-spectral imagery to estimate soil alkalinity and salinity over a large area. Bannari *et al.* [34] found that the shortwave infrared (SWIR) range was superior in detecting soil salinity and sodicity, and two indices from the EO-1 ALI image were built to differentiate slightly and moderately saline and sodic soils. Fan *et al.* [35] estimated soil salinity from the ALI-convolved field spectra in the Yellow River Delta in China.

The aim of this study is to investigate the potential of mapping soil alkalinity and salinity from the Landsat 8 OLI image assisted with soil physico-chemical measures and spectra in northern Songnen Plain. In order to select sensitive bands to soil pH and EC, physico-chemical and spectral analyses of soil samples were conducted. Relationships between spectral reflectance and soil alkalinity and salinity were then explored in stepwise regression models. The models were finally modified and applied to the OLI image to map soil alkalinity and salinity in the study area.

2. Materials and Methods

2.1. Study Area

The Wuyu'er-Shuangyang River Basin is located in northern Songnen Plain, covering an area of 23,000 km^2. There are several towns of Fuyu, Yi'an, Baiquan, Keshan, and Bei'an in the basin (Figure 1). The climate is temperate monsoon continental with annual average precipitation and temperature approximately 415 mm and 3.2 °C, respectively. The mean elevation is about 207 m. Its northeast border is hilly upland and the southwest border is wetland. Terrain of the study area is low and flat dominated with cultivated lands. Within this closed-flow basin, two ephemeral rivers, the Wuyu'er River and Shuangyang River wander through the central area and flow into the Zhalong wetland in the south (Figure 1). Grasslands distribute near the rivers and the wetland. The basin contains six soil types defined in the FAO-90 Revised Soil Classification System (Figure 2). Phaeozems and chernozems are the primary soils in the basin, characterized as dark color and high soil organic matter content. Different degrees of saline-alkali soils are also found in the basin.

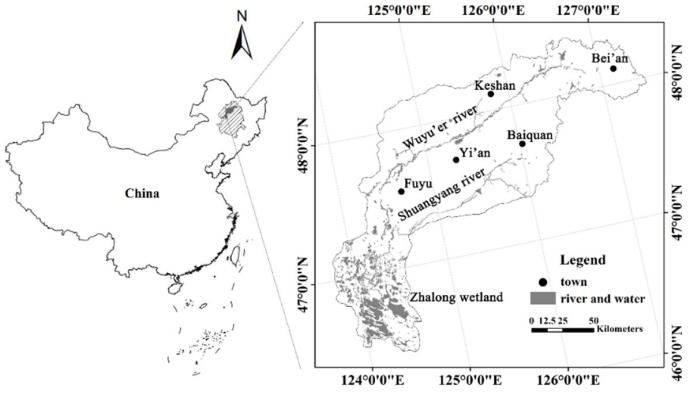

Figure 1. The Wuyu'er-Shuangyang River Basin in the Songnen Plain, Northeast China.

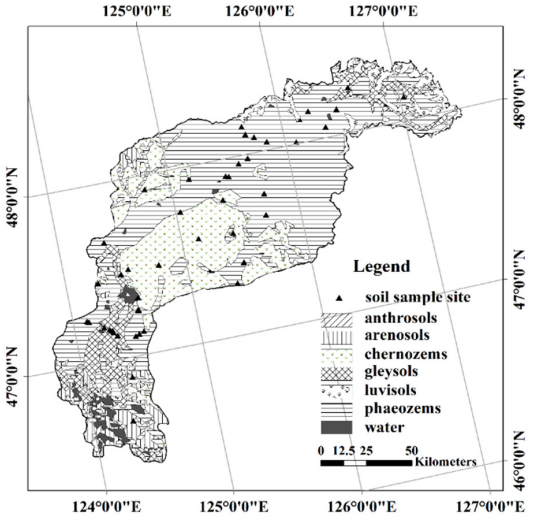

Figure 2. Soil types of the study area and distributions of soil sample sites.

2.2. Data Sets and Preprocessing

2.2.1. Soil Samples and Preprocessing

As shown in Figure 2, a total of 59 soil sampling sites were collected in the period of October 2013 to May 2015. The triangular cluster plot approach was applied to collect soil samples [20]. At each site four samples were collected. In grasslands with relatively homogeneous grass covers, one sample was collected at the central point and the other three were spread 30 meters away surrounding the central point. In cultivated lands, the four points were the corners of a 20-m rectangle. The GPS locations of all sample points were recorded. All soil sample data sets are listed in Table 1. In total, 221 topsoil samples were collected at 45 of the 59 soil sample sites. Spring was the optimal season for estimating soil alkalinity and salinity because of salt accumulation in the topsoil and limited vegetation cover. Among these, 113 samples collected in spring (April and May) of 2014 and 2015 were used to calibrate and validate the predictive models. 108 (the rest of 221) samples collected in autumn of 2013 were used to analyze soil physico-chemical properties, providing basic information for further spectral analysis. Fourteen soil samples in the rest (14 of 59) sites were collected on 26 April 2014 and 5 May 2014, close to the dates of the OLI image acquisition. These samples were used to perform an accuracy assessment of the OLI-derived alkalinity and salinity. These 14 sample sites were widely distributed in the study area and in different degrees of saline-alkali soils. All samples were air-dried, grounded and put through 2-mm sieves [36] to remove water, large debris, stones, and stubble before physico-chemical and spectral analysis.

Table 1. Soil sample data sets used in this study.

Data sets	Samples	Types	Time	Measurements
Spectral properties analysis and predictive model building	113	cultivated lands and grasslands	spring 2014, 2015	pH, EC, spectra
Soil properties analysis	108	cultivated lands and grasslands	Autumn 2013	pH, EC, contents of eight ions, ESP
Accuracy assessment of image inversion	14	cultivated lands and grasslands	spring 2014	pH, EC

2.2.2. Soil Spectra and Preprocessing

Lab spectra of soil samples were recorded with the SVC (Spectra Vista Corporation, USA) HR 1024i field spectrometer in the 350–2500 nm spectral range with sampling intervals of 3.5 nm (350–1000 nm), 9.5 nm (1000–1850 nm), and 6.5 nm (1850–2500 nm). Spectra of the air-dried, grounded, and sieved soil samples were measured in lab with natural sunlight at 10:00 AM to 14:00 PM in clear days. Instead of in-field spectral measurement, our method reduced spectral noises from soil water, roughness and debris [37] and therefore, the recorded spectra were primarily related to soil's physico-chemical properties that we explored in this study. Dishes of 7.5 cm diameter and 2 cm depth were overfilled with soil and laid on a black background cloth. With the SVC spectrometer, spectral signatures (350–2500 nm) were collected at a height of 10 cm above soil surface at a nadir position and 25° field of view (FOV). For each sample, five reflectance spectra were measured and averaged into one spectral curve with the SVC HR 1024i PC data acquisition software. Spectra were smoothed and then regions matching each OLI image band were re-sampled to represent the corresponding OLI band.

2.2.3. Soil Physico-Chemical Measurement

Each soil sample was put through 1-mm sieves and mixed with deionized water. After shaking, centrifuging and filtering, clear soil-water mixtures were used for physico-chemical measurement. The pH of the 1: 2.5 soil-water mixtures [38] was measured with the pH Meter (LEICI PHSJ-5). The EC of the 1:5 soil-water mixtures [18] was measured with the Conductivity Salinity Meter (LEICI DDS-307) and transformed into the 25 °C equivalents. Contents of eight ions were also measured in the 1:5 soil-water mixture: K^+, Na^+, Ca^{2+} and Mg^{2+} were measured with the inductively coupled plasma optical emission spectrometer (ICP-OES); $CO_3{}^{2-}$ and $HCO_3{}^-$ were measured with the hydrochloric acid (HCl) method; $SO_4{}^{2-}$ was measured with the ethylene diamine tetraacetic acid (EDTA) complexometric titration method and Cl^- was measured with silver nitrate ($AgNO_3$) titration method. Finally, the ESP was measured with the exchange method using the ammonium acetate-ammonium hydroxide [39] and the ICP-OES.

2.2.4. Satellite Imagery and Preprocessing

Satellite images from the Landsat 8 OLI were used in this study. The OLI imagery has seven multi-spectral bands in VIS-SWIR region at 30-m spatial resolution [40]. In comparison with other Landsat systems (TM and ETM+), the OLI has a new "deep blue" band, which may provide additional information about soil properties in this study.

Three OLI images acquired on 17, 30 April and 3 May 2014 covering the study area were downloaded at the United States Geological Survey (USGS) GloVIS Data Center [41]. At this time, vegetation has not started to grow in this cold region and therefore, its effects on soil spectra were limited. The images were geo-referenced using 30 ground control points selected from the 1:50,000 topographic maps, reaching a root-mean-square error less than half pixel. For atmospheric correction, the Fast Line-of-Sight Atmospheric Analysis of Spectral Hypercubes (FLAASH) module was used to convert digital numbers to surface reflectance. The FLAASH model incorporates the MODTRAN 4

radiation transfer functions to calculate the atmospheric interference of land-reflected signals relying on built-in aerosol models [42]. Kruse [43] found that the FLAASH-corrected reflectance spectra were generally similar and matched to that of field image spectra within approximately 5% absolute reflectance at most wavelengths in the 400–2500 nm spectral range. In this study, the OLI images were atmospherically corrected with the FLAASH in ENVI 5.1 software.

Vegetation atop of soil surface reduces the sensitivity of remote sensing signals to soil. Here we adopted the thresholding of the normalized difference vegetation index (NDVI) to identify non-soil pixels. Following other studies [32,44], pixels with NDVI > 0.3 were assumed vegetated. Snow, ice, and water bodies were identified with NDVI < 0.05. Other land cover types, such as paddy fields, residential, and roads were masked via visual interpretation. Only bare soil pixels were examined in this study.

2.3. Methodological Approach

Correlation analysis was performed to detect spectral sensitivities to the physico-chemical variables of soil. Correlation coefficient is a measure of the strength and direction of the relationship between two variables [45]. The 0.05 probability level was used to test the significance of the correlation.

The statistically sensitive bands were then used to establish stepwise regression models to extract soil alkalinity and salinity. The coefficient of determination (R^2), adjusted R^2 (R^2_{Adj}), and RMSE were calculated to evaluate the validity of the modeling process. The R^2 explains the goodness of fit between the predicted and observed values. The R^2_{Adj} adjusts the over-fit of the regression. The RMSE indicates the absolute estimation error. These metrics can be calculated as:

$$R^2 = 1 - \frac{\sum_{i=1}^{n} (Y - Y')^2}{\sum_{i=1}^{n} (Y' - \overline{Y})^2} \quad (1)$$

$$R^2_{adj} = 1 - \frac{n-1}{n-k-1}(1 - R^2) \quad (2)$$

$$RMSE = \sqrt{\frac{\sum_{i=1}^{n} (Y - Y')^2}{n}} \quad (3)$$

where Y and Y' are measured and predicted values, respectively. $\overline{Y}$ is the average of observed values, n is the number of observation and k is the number of variables.

Collinearity from the closely inter-related variables may lead to an unpractical model and high prediction errors. In this study, it seems inevitable in the regression because reflectance among different spectral bands is highly inter-related. Here the variance inflation (VIF), condition index, and proportion of variation were used to examine the collinearity in the regression model. The VIF is the reciprocal of tolerance that determines to what extent the independent variables are linearly related to one another. The condition indices are the square roots of the ratios of the largest eigenvalue to each successive eigenvalue. The proportion of variation is the percentage of the variance of the variable that is associated with the eigenvalue [46,47]. In this study, the thresholds of VIF > 10, condition index > 30 and proportion of variation > 50% were used to define the collinearity.

3. Results

3.1. Salinity and Alkalinity Properties of Soil Samples

It is commonly accepted that soil with pH above 7.5 is considered alkaline [15,16]. As shown in Table 2, the pH values of all samples ranged from 5.34 to 10.72, with an average of 7.92 and median of 8.00. Therefore, most soils in the study area were alkaline. The EC values ranged from 0.05 dS/m to 17.80 dS/m, with an average of 0.76 dS/m and a median of 0.28 dS/m. An EC threshold of 4 dS/m is

commonly accepted as the boundary between saline and non-saline soils [31]. Most soils in the study area were characterized as non-saline soils.

Table 2. Descriptive statistics of soil physico-chemical measurements.

Data-Set	Mean	Maximum	Minimum	SD	Median	Confidence Interval *
pH	7.92	10.72	5.34	1.65	8.00	7.68–8.16
EC (dS/m)	0.76	17.80	0.05	1.76	0.28	0.51–1.00
SO_4^{2-} (mg/L)	284.32	522.43	3.72	115.63	283.81	266.41–302.24
HCO_3^- (mg/L)	147.68	1507.00	55.57	120.26	127.86	129.05–166.32
CO_3^{2-} (mg/L)	47.62	314.52	0	90.03	0	33.67–61.57
Na^+ (mg/L)	154.94	808.50	7.28	132.34	129.23	134.43–175.44
K^+ (mg/L)	7.41	28.89	3.06	3.55	6.45	6.87–7.96
Ca^{2+} (mg/L)	116.85	177.80	43.45	23.94	112.75	113.15–120.56
Mg^{2+} (mg/L)	16.90	59.85	4.78	7.37	15.64	15.76–18.04

* Significant at the 0.05 probability level.

Alkalinization and salinization are resulted from concentration of water-soluble salts in soils. The contents of the eight ions of soil samples may reveal further information about soil alkalinity and salinity in the study area. As shown in Table 2, the predominant anions were SO_4^{2-} and HCO_3^-, and the predominant cations were Na^+ and Ca^{2+}. The Cl^- was not found in our soil samples and therefore, was not examined hereafter.

A correlation matrix (pearson's r) was created to examine the relationships between the physico-chemical variables (Table 3). The relationships between pH and two ions (CO_3^{2-} and Na^+) were highly positive (0.88 and 0.81), indicating the presence of alkaline soils in the study area. The soluble salts containing SO_4^{2-} are neutral, while alkaline sodic soils contain Ca^{2+} as $CaCO_3$ that is insoluble at high pH [48]. The Na_2CO_3 (sodium carbonate) and $NaHCO_3$ (sodium bicarbonate) were alkaline soluble salts that contributed to soil alkalinity in the study area. The correlation coefficient between pH and HCO_3^- was low (0.18). The pH value of Na_2CO_3 solution was higher than that of $NaHCO_3$ solution even though they had the same amount of substance. Therefore, CO_3^{2-} was better than HCO_3^- in explaining high pH in spite of low content. High correlation (0.81) between Na^+ and pH in Table 3 also suggests that Na^+ was another important variable to explain soil alkalinity. High correlation between Na^+ and CO_3^{2-} (0.86) suggests that Na_2CO_3 was the main solute salt contributing to soil alkalinity. The correlation coefficient between EC and pH was high (0.77). Moreover, the relationships between EC and two ions (CO_3^{2-} and Na^+) were very high, reaching 0.87 and 0.93, respectively. These indicated that soil salinity was highly correlated with its alkalinity in the study area. The correlation coefficient between EC and Na^+ was higher than that between pH and Na^+, which suggested other non-alkaline salts contributing to EC.

Table 3. The correlation matrix among pH, EC, and salt ions.

Data-set	EC	pH	SO_4^{2-}	HCO_3^-	CO_3^{2-}	Na^+	K^+	Ca^{2+}	Mg^{2+}
EC	1								
pH	**0.77 ***	1							
SO_4^{2-}	−0.17	−0.26	1						
HCO_3^-	0.25	**0.18**	0.0006	1					
CO_3^{2-}	**0.87 ***	**0.88 ***	−0.32	0.15	1				
Na^+	**0.93 ***	**0.81 ***	−0.17	0.33*	**0.86 ***	1			
K^+	−0.12	−0.23	0.17	−0.09	−0.05	−0.15	1		
Ca^{2+}	−0.32	−0.39 *	0.41 *	−0.04	−0.28	−0.31 *	0.48 *	1	
Mg^{2+}	0.13	0.21	0.32	−0.04	0.19	0.09	0.35	0.35	1

* Significant at the 0.05 probability level.

Alkalinization, the increase of pH of soil, is associated with sodification in which Na^+ is the main salt of salinization and is the typical characteristics of sodic soils [1]. Soluble carbonate in the form of Na_2CO_3 and $NaHCO_3$ usually appears at high pH (>8.4) and enhances soil sodicity [49]. In this study, the HCO_3^- was detected in all samples but CO_3^{2-} was only observed in 44 samples that had high pH values. The ESP measurements were used to test soil sodicity. Among soil samples with pH > 8.5, there were 11 samples with ESP values higher than 15, showing that there were sodic soils in the study area and the sodification was associated with high pH values.

3.2. Spectral Properties of Sample Soils

For demonstration purpose, spectra curves of all soil samples were categorized into five soil alkalinity (pH) levels and four soil salinity levels (EC). Five soil alkalinity levels are strongly alkaline (pH > 9.5), moderately alkaline (9.5 > pH > 8.5), slightly alkaline (8.5 > pH > 7.5), moderate (7.5 > pH > 6.5), and acidic (pH < 6.5) as described in Song [16]. As well, four soil salinity levels are strongly saline (EC > 16 dS/m), moderately saline (16 dS/m > EC > 8 dS/m), slightly saline (8 dS/m > EC > 4 dS/m), and non-saline (EC < 4 dS/m) as described in Metternicht and Zinck [24]. In combining these two soil properties, all soil samples were finally categorized into seven pH-EC levels: unaffected soils (pH < 7.5, EC < 4 dS/m), slightly alkaline and non-saline, moderately alkaline and non-saline, strongly alkaline and non-saline, strongly alkaline and slightly saline, strongly alkaline and moderately saline, and strongly alkaline and strongly saline. Spectra of soil samples in each class were averaged into one average spectrum and demonstrated in Figure 3.

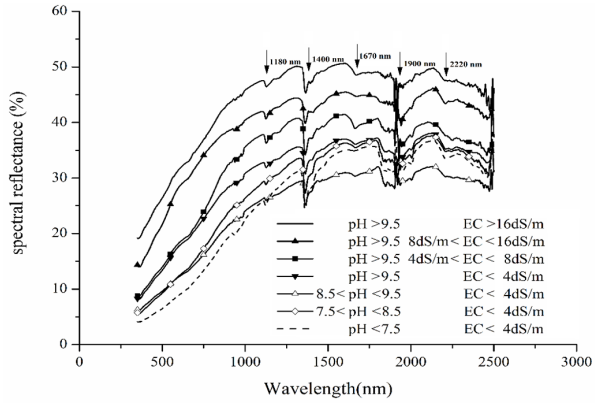

Figure 3. Average soil spectra at 1 nm interval for soil samples with seven pH-EC levels.

Figure 3 illustrates spectral characteristics of different soil alkalinity and salinity classes. Generally, spectral curves of soils had similar shapes, with increasing reflectance from VIS to NIR and remaining high reflectance in SWIR. The exceptions were two distinct wavy troughs and three slight absorption troughs. The two distinct wavy troughs were near 1400 nm and 1900 nm from water absorption. These should be counted as noises from water vapors in air and moisture residue in air-dried soils. The three slight absorption troughs were near 1180 nm, 1670 nm, and 2220 nm. At shorter wavelengths (VIS-NIR), acid soils (pH > 6.5) had apparently lower reflectance than alkaline soils (pH > 7.5) and strongly alkaline soil had higher reflectance than moderately and slightly alkaline soils. The trends were disturbed at SWIR range.

With all soil samples, the correlation coefficients between pH, EC, and the 1-nm lab spectral reflectance were calculated (Figure 4). The two water absorption bands near 1400 nm and 1900 nm were excluded. The correlation coefficients in VIS-NIR ranges were very high (0.84) although there was a decreasing trend in SWIR (0.23). The correlation coefficients of pH were higher than that of EC in almost all VIS and NIR wavelengths but the trend was reversed in SWIR wavelengths. The bands with largest correlation coefficients to pH and EC were 475 nm (0.84) and 354 nm (0.84), respectively.

The largest correlation coefficients to pH in three slight absorption troughs were 0.59, 0.23, and 0.28 (1180, 1670, and 2205 nm). For EC, the largest correlation coefficients in three slight absorption troughs were 0.63, 0.41, and 0.40 (1180, 1670, and 2209 nm).

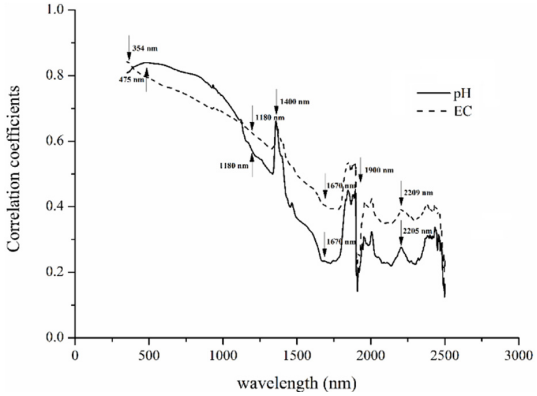

Figure 4. Correlation coefficient curves between pH, EC, and soil spectra at 1nm interval.

3.3. Sensitivity of Broad Band Reflectance

The narrow band spectral features in Figure 3 and their relationships with pH and EC in Figure 4 may not be easily detected in broad band satellite imagery. In order to assess the sensitivity of broad band reflectance to soil alkalinity and salinity, we resampled all lab spectra of soil samples into the bandwidths of the 7-band OLI image and re-calculated the correlation coefficients (Table 4).

Table 4. Pearson correlation coefficients between pH, EC, and the resampled broad band reflectance (matching band1 -7 of the OLI image).

Data-Set	pH	EC	b1	b2	b3	b4	b5	b6	b7
pH	1								
EC	0.51 *	1							
b1	**0.82** *	**0.78** *	1						
b2	**0.82** *	**0.77** *	1 *	1					
b3	**0.81** *	**0.75** *	1 *	1 *	1				
b4	**0.79** *	0.72 *	0.98 *	0.99 *	1 *	1			
b5	0.73 *	0.66 *	0.94 *	0.95 *	0.98 *	0.97 *	1		
b6	0.30 *	0.41 *	0.62 *	0.62 *	0.64 *	0.66 *	0.77 *	1	
b7	0.26 *	0.35 *	0.54 *	0.54 *	0.56 *	0.58 *	0.67 *	0.96 *	1

* Significant at the 0.05 probability level.

After resampling, the coefficients between pH, EC, and 7 OLI-like bands were slightly lower than those of narrow band spectra, and a decreasing trend was also observed from band 1 to band 7. As highlighted in the Table 4, the correlation coefficients between pH and the first four bands were higher than 0.75. The correlation coefficients between EC and the first three bands were higher than 0.75. These bands with higher correlations were potentially sensitive bands to detect soil alkalinity and salinity. Strong correlations between these broad bands were also clear, indicating collinearity between these bands.

3.4. Stepwise Regression for Estimating Soil pH and EC

Soil pH and EC were estimated with the stepwise regression models. When developing each model, soil samples were randomly divided into a calibration set (two-thirds) and a validation set (one-third). The calibration set was used to build the model and the validation set was to evaluate the accuracy of predicted results. The variables in a stepwise regression model can be kept only when all of the three thresholds meet: VIF > 10, condition index > 30, and proportion of variation > 50%.

Finally, at the 0.05 significant level, only band 2 and band 6 were found contributing to the regression model for pH prediction. Other bands were eliminated in the stepwise process because of their strong collinearity. Similarly, only band 1 contributed to EC prediction. The models were described as:

$$pH = 7.84 + 0.46b2 - 0.12b6 \quad (4)$$

$$EC = -3.35 + 0.56b1 \quad (5)$$

where b1, b2, and b6 were reflectance of the resampled, OLI-like band 1, band 2, and band 6, respectively.

Detailed descriptive statistics of both models are listed in Table 5. The values of R^2 and R^2_{Adj} of calibration set revealed high goodness-of-fit of the two models. For pH prediction, the VIF, condition index and proportion of variation (Table 5) confirmed that there was no clear collinearity between the two bands in Equation (4). With the validation set, the values of R^2 were 0.75 and 0.52. The two values were comparable with those of calibration set. The RMSE of pH reached 0.98 and that of EC reached 1.07 dS/m, respectively. These indicated that the two models could be used to estimate soil alkalinity and salinity. But the slope values were 0.61 and 1.49, which indicated underestimation of soil alkalinity and overestimation of soil salinity.

Table 5. Performance statistics of the stepwise regression models to estimate pH and EC.

Model	Calibration Set		Collinearity Diagnostics			Validation Set		
	R^2	R^2_{Adj}	Variance Inflation	Proportion of Variation	Condition Index	RMSE	R^2	Slope
pH	0.74	0.73	2.11	45.77% 99.26%	18.94	0.98	0.75	0.61
EC	0.73	0.72	-	-	-	1.07 dS/m	0.52	1.49

3.5. Soil EC and pH Distributions in the Study Area

With the two models above, the pH and EC distributions were derived from the OLI images as shown in Figures 5 and 6. The non-soil area, which was mostly water (6.12%), developed lands (4.34%), and green vegetation (17.10%) with NDVI > 0.3, covered 27.56% of the basin and was masked out in this study. A small piece of the area in the west end of the basin (2.43%) was not covered in the OLI image.

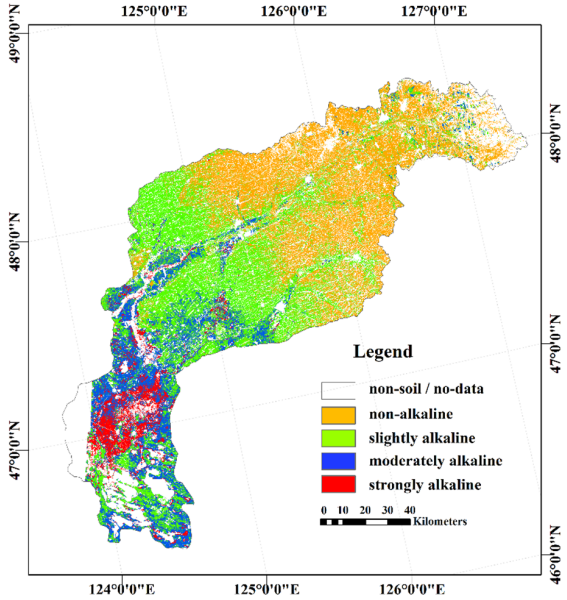

Figure 5. Spatial distribution of soil alkalinity across the basin.

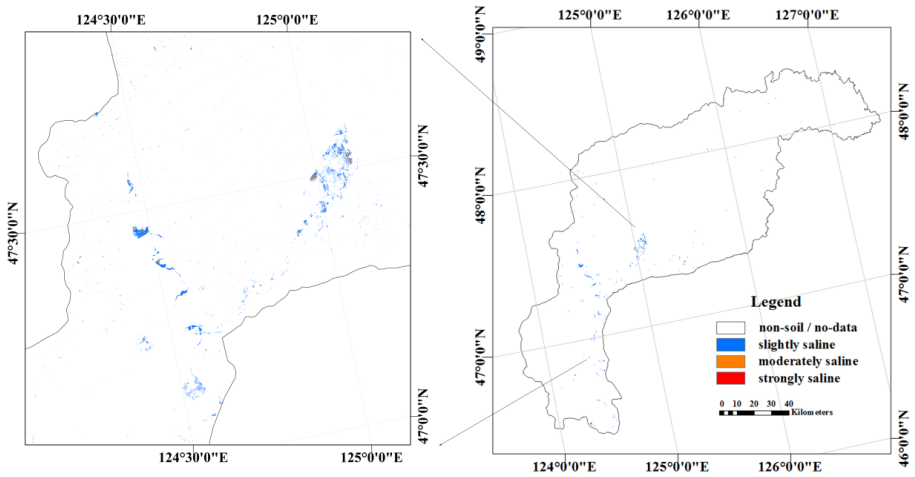

Figure 6. Distributions of soil salinity across the basin.

As shown in Figure 5, non-alkaline soils (pH < 7.5) cover 25.55%, and alkaline soils (slight, moderate, strong) are 44.46% of the basin. Therefore, soil alkalinity was an important characteristic in the study area. Geographically, it varied from low to high across the northeast to southwest of the basin. This trend agreed with the landscape of the study area, suggesting that soil alkalinity came from parent rocks and became concentrated nearby the Zhalong wetland and downstream low elevations in the south.

For the estimated EC values, most areas of the basin were dominated with non-saline soils (Figure 6). In Figure 6, saline soils were nearly the Zhalong wetland and rivers with limited physical accessibility. The saline soils only covered 0.23% of the basin. Among all saline soil pixels, those in the slightly saline level were 0.21% and those in the moderately saline level were 0.02% in the basin. Strongly saline soil was only 0.0006% in the basin and could not be clearly displayed in the figure. This suggested that soil salinization was not a big concern in the basin. Comparing Figures 5 and 6 saline soils were also strongly alkaline, but strongly alkaline soil was not necessarily highly saline. Areas of soil salinization (saline-alkali soils) were distributed between the wetland and downstream of the two rivers sporadically, as well as in the north of the Shuangyang River.

Accuracies of the two figures were assessed with pH and EC measurements at the 14 soil sample sites, reaching the RMSE of 1.01 for pH estimation and 0.64 dS/m for EC estimation in the study area.

4. Discussion

4.1. Soil Characteristics of the Study Area

The physico-chemical and spectral analyses of soil in the Wuyu'er-Shuangyang River Basin provided fundamental information for understanding soil properties and developing statistical models to estimate soil alkalinity and salinity from satellite imagery. The pH and EC analysis showed that most soils in the watershed were alkaline. Saline soils were also alkaline soils but their distributions were rare in the study area. The ESP measurements showed there was slight sodification in the study area. These reflected typical characteristics of soda saline-alkali soils in the Songnen Plain. The contents of HCO_3^-, CO_3^{2-}, and Na^+ were high and their contributions to soil alkalinity and salinity were also high. However, SO_4^{2-} was an exception. The content was high but the contribution to soil salinity was low, which deserves further exploration in future research.

4.2. Potential Use of Soil Spectra for Soil Alkalinity and Salinity Retrieval

Spectral analysis revealed high correlation between spectral reflectance and physico-chemical properties of soil in the VIS-NIR-SWIR spectral region. The correlation coefficients in VIS and NIR

bands were higher than those in SWIR bands. Our findings were in agreement with Ong and Cudahy [31], Lopez-Granados *et al.* [50], and Stoner [51] who found that spectral variations in 350–1200 nm were highly related to the changes of the soil pH, and the relationships were much higher in shorter wavelengths. According to Bear [52], organic matter, water, and oxidation were influencing factors of pH and color association. For air-dried soil used in this study, the primary influence was organic matter. According to Liu *et al.* [33], the pH and EC had negative relation with organic matter of soda saline-alkali soil in the west of Jilin province that was part of Songnen plain. Moreover, the positive relationship between pH and EC in our study agreed with the above-mentioned studies. Solution of alkaline salts results in high pH and declines the organic matter in soda saline-alkali soil [33], which further affects the color of soda saline-alkali soil [53]. The shorter VIS wavelength has an advantage to reflect the variation of soil color than longer wavelengths. Similarly, our study found good relationships between EC and spectral reflectance especially in shorter wavelength bands.

Oppositely, Bannari *et al.* [34] found that the SWIR range had higher advantages than VIS and NIR in detecting soil salinity and sodicity. Similar result could be found in other research [24]. The sodicity classes in Bannari *et al.* [34] were lower than those of our study. Soil salinity was highly related to soil alkalinity that influenced soil organic matter as mentioned above. This might be the reason that high alkaline and saline soils in our study area were better distinguished in VIS than longer wavelengths.

Moreover, the average spectral curve of slightly saline soil was close to that of highly alkaline soil in VIS wavelengths, making it difficult to distinguish between these two soils in this spectral region. Similar observations could be found in [37,54]. This might result in estimating error of soil EC because the EC model in our study was constructed using OLI band 1. This error is not a big concern in this study area because of the limited coverage of saline soils.

4.3. Potential Use of OLI Image for Soil Alkalinity and Salinity Retrieval

Assisted with intensive lab spectra of soil samples, our study tested the feasibility of the Landsat 8 OLI image in mapping soil alkalinity and salinity. Past studies (e.g. Fan *et al.* [35]) reported that soil alkalinity/salinity retrieval with broad band imagery may become questionable due to its insufficient spectral resolution. The OLI image has relatively narrower bandwidths than other Landsat systems such as TM and ETM+, which may be superior in soil alkalinity/salinity inversion. In our results, although correlation coefficients became lower due to band aggregation, significantly high relationships were observed between OLI bands and soil pH and EC. Among the OLI bands, band 2 (blue) had the highest correlation to pH (0.82) and band 1 (deep blue) had the highest correlation to EC (0.78), which were comparable with 1-nm lab spectra of 475 nm (0.84) and 354 nm (0.84). Therefore, OLI image could be applied to map soil alkalinity and salinity in a large spatial extent.

OLI band 2 and 6 that were selected in a stepwise regression model to estimate soil pH. From the regression coefficients, the band 2 was a primary variable, indicating the collinearity between the two bands was very slight. The stepwise regression model to estimate soil EC was constructed with OLI band 1 and was a single variable regression indeed. Equation (4) could estimate soil pH from acidic to high alkaline. Equation (5) could estimate soil EC from very slightly content to very high content (non-saline to high saline). Both models reached fairly good accuracies. These also indicated the feasibility of the stepwise regression models in estimating soil alkalinity and salinity in the study area as well as the Songnen Plain in a larger extent. As for the season, spring was the optimal season for estimating soil alkalinity and salinity because of salt accumulations and limited vegetation. Models derived from soil samples in spring might result in uncertainties when they are applied to images acquired in other seasons.

It should be noted, however, lab spectra in our study were measured under ideal conditions where the effects of soil roughness, moisture, and vegetation remnants were removed. These effects *in situ* may result in underestimation in OLI-based assessment. The dry spring condition in our study sites was characterized with low soil moisture and limited impacts from green vegetation and geomorphology. Although these are not directly comparable with lab-measured physical-chemical soil

characteristics, we consider this is the best comparison that can be done in this study. Furthermore, reflectance of the OLI band 1, at its short wavelength of deep blue, is strongly affected by atmospheric scattering and absorption. Therefore, atmospheric correction of the OLI imagery is mandatory for reasonable retrieval of soil salinity. Recent release of Landsat 8 OLI products includes the surface reflectance data sets [41]. If this product is proven atmospherically corrected, it may be better applied in soil alkalinity and salinity mapping than other satellite images.

4.4. Geographic and Land Use Consideration of Soil Alkalinity and Salinity

The study basin is part of the Songnen Plain in the Northeast China, a typical saline-alkali soils region. Our results suggested that soil alkalinity in the plain was strong and widespread, but soil salinity was less dominant and was accompanied with alkalinization. The most strongly alkaline and saline-alkali soils were close to the Zhalong wetland and the downstream of rivers. According to Wang *et al.* [1], the distribution of soil salinity and alkalinity is affected by geomorphic structure. Alkalinization often occurs in the lower landscapes, such as rivers and closed-flow areas, where ground water is rich in carbonates of sodium and other salts. These areas are mostly pastures and croplands. Strong soil alkalinization and crop productivity degradation should be taken into serious consideration for sustainable agricultural management. Nevertheless, soil dynamics and different agricultural managements should not be neglected in such an important agricultural region. With the framework initialized in this preliminary study, further investigations will be conducted to explore the sensitivity and uncertainty of remote sensing-assisted soil mapping at a regional scale. The dynamics of soil alkalinization and salinization in spatial scale and the driving forces in temporal scale are our focuses in future study.

5. Conclusions

This study conducted soil spectral and physico-chemical analyses and developed the stepwise regression models to map soil alkalinity and salinity using the OLI image. With soil spectra, good correlations between pH, EC, and the 1-nm reflectance were observed. After band aggregation, the OLI-estimated pH and EC distributions reached the adjusted R^2 values of 0.73 and 0.72, respectively. Alkaline soils (pH > 7.5) covered 44.46% of the basin, coming from the dominant salt ions of Na^+, HCO_3^-, and CO_3^{2-} in parent rocks. The saline soil (EC > 4 dS/m) only covered 0.23% of the basin and was actually saline–alkali soil. However, saline soils should not be ignored in the study area because soil salinization is accompanied by soil alkalinization. The alkaline soils and saline–alkali soils were mostly distributed in the low-elevation areas nearby the Zhalong wetland and downstream of rivers. Our findings indicated the feasibility of estimating soil alkalinity and salinity from the OLI imagery. The approaches developed in this study were useful to extract spatial distributions of soil properties in the Songnen Plain, Northeast China, which may provide useful information for further assessment of soil alkalinization and salinization over space and time in such an important agricultural region.

Acknowledgements: This study was financially supported by the Key Provincial Natural Science Foundation of Heilongjiang Province (No. ZD201308); the Doctoral Innovational Programs Foundation of Harbin Normal University of China (HSDBSCX 2013-01); the National Natural Science Foundation of China (No. 41371397); the National Natural Science Foundation of China (No. 41201183) and the Science and Technology Project Foundation of Heilongjiang Province Education Department (No. 12531209).

Author Contributions: Lin Bai, Cuizhen Wang, and Shuying Zang conceived and designed the experiments and methodology; Lin Bai, Qiannan Hao, Yuhong Zhang, and Yuexiang Wu collected data; Lin Bai analyzed the data and developed the model; Lin Bai and Cuizhen Wang wrote the manuscript.

Conflicts of Interest: The authors declare no conflict of interest.

References

1. Wang, L.; Seki, K.; Miyazaki, T.; Ishihama, Y. The causes of soil alkalinization in the Songnen Plain of Northeast China. *Paddy Water Environ.* **2009**, *7*, 259–270. [CrossRef]

2. Metternicht, G. Assessing temporal and spatial changes of salinity using fuzzy logic, remote sensing and GIS: Foundations of expert system. *Ecol. Model.* **2001**, *144*, 163–179. [CrossRef]
3. Wang, R.Z.; Li, J.D. Dynamic population models of the ecological dominance during the deterioration of Leymuschinensis grassland. *ActaPhytoecol Sin.* **1995**, *19*, 170–174. (In Chinese).
4. Li, X.J. The alkili-saline land and agricultural sustainable development of the Western Songnen Plain in China. *SciGeogr Sin.* **2000**, *20*, 51–55.
5. Lin, N.F.; Bounlom, V.; Tang, J.; Bian, J.M. Study on the relation between the formation of saline-alkali soil and the neotectonic movement. *Global Geol.* **2005**, *24*, 282–288.
6. Wu, L.Z.; Li, Q.S. Research of mechanism of saline desertification in Western Songnen Plain. *Soil Water Conserv.* **2003**, *17*, 79–81.
7. Wang, R.Z.; Gao, Q.; Chen, Q. Effects of climatic change on biomass and biomass allocation in Leymuschinensis (Poaceae) along the North-east China Transect (NECT). *J. Arid Environ.* **2003**, *54*, 653–665.
8. Wang, F.S.; Tian, Z.C. The groundwater effect in the process of soil salinization of the Songnen Plain, Jilin province. *Jilin Geol.* **2002**, *21*, 79–87.
9. Zhang, D.F.; Wang, S.J. Mechanism of freeze-thaw action in the process of soil salinization in northeast China. *Environ. Geol.* **2001**, *41*, 96–100. [CrossRef]
10. Qiu, S.W.; Zhang, B.; Wang, Z.C. Analyses on current situation, causes of formation, and way of management of desertification in western Northeast Plain of China. *Quat. Sci.* **2005**, *25*, 63–73.
11. Fauck, R. Influences of agriculture practices on soil degradation. *FAO Soil Bulletion. UN.* **1977**, *34*, 83–84.
12. Schipper, L.A.; Sparling, G.P. Performance of soil condition indicators aross taxonomic groups and land uses. *Soil Sci. Soc. Am. J.* **2000**, *64*, 300–311. [CrossRef]
13. Csillag, F.; Pásztor, L.; Biehl, L.L. Spectral band selection for the characterization of salinity status of soils. *Remote Sens. Environ.* **1993**, *43*, 231–242. [CrossRef]
14. Buckman, H.O.; Brady, N.C.; Weil, R.R. *The Nature and Properties of Soils*; Prentice Hall: Englewod Cliffs, NJ, USA, 2002.
15. Richards, L.A. Diagnosis and improvement of saline and alkali soils. *Soil Sci.* **1954**, *78*, 154–155. [CrossRef]
16. Song, H.Y. *Detection in Near-Infrared Spectroscopy of Soils*; Chemistry Industry Press: Beijing, China, 2013.
17. Corwin, D.L.; Lesch, S.M. Application of soil electrical conductivity to precision ag-riculture: Theory, principles, and guidelines. *Agron. J.* **2003**, *95*, 455–471. [CrossRef]
18. Rhoades, J.D. *Soluble Salts*; ASA and SSSA: Madison, WI, USA, 1982.
19. Dwivedi, R.S. Monitoring of salt-affected soils of the Indo-Gangetic alluvial plains using principal component analysis. *Int. J. Remote Sens.* **1996**, *17*, 1907–1914. [CrossRef]
20. Fallah Shamsi, S.R.; Zare, S.; Abtahi, S.A. Soil salinity characteristics using moderate resolution imaging spectroradiometer (MODIS) images and statistical analysis. *Arch. Agron. Soil Sci.* **2013**, *59*, 471–489. [CrossRef]
21. Lobell, D.B.; Lesch, S.M.; Corwin, D.L.; Ulmer, M.G.; Anderson, K.A.; Potts, D.J.; Doolittle, J.A.; Matos, M. Regional-scale assessment of soil salinity in the Red River Valley using multi-year MODIS EVI and NDVI. *J. Environ. Qual.* **2010**, *39*, 35–41. [CrossRef] [PubMed]
22. Rao, B.R.M.; Dwivedi, R.S.; Venkataratnam, L.; Ravishankar, T.; Thammappa, S.S.; Bhargawa, G.P.; Singh, A.N. Mapping the magnitude of sodicity in part of the Indo-Gangetic Plains of Uttar Pradesh, Northern India using Landsat-TM data. *Int. J. Remote Sens.* **1991**, *12*, 419–425. [CrossRef]
23. Wu, H.S.; Liu, Z.L. Remote sensing and mapping of saline sodic land based on spectral characteristics for Da'an city. *Syst. Sci. Compr. Stud. Agric.* **2007**, *23*, 178–182.
24. Metternicht, G.; Zinck, J.A. Spatial discrimination of salt- and sodium-affected soil surfaces. *Int. J. Remote Sens.* **1997**, *18*, 2571–2586. [CrossRef]
25. Metternicht, G.I. Categorical fuzziness: A comparison between crisp and fuzzy class boundary modelling for mapping salt-affected soils using Landsat TM data and a classification based on anion ratios. *Ecol. Model.* **2003**, *168*, 371–389. [CrossRef]
26. Dwivedi, R.S.; Sreenivas, K. Image transforms as a tool for the study of soil salinity and alkalinity dynamics. *Int. J. Remote Sens.* **1998**, *19*, 605–619. [CrossRef]
27. Kalra, N.K.; Joshi, D.C. Potentiality of Landsat, SPOT and IRS satellite imagery, for recognition of salt affected soils in Indian Arid Zone. *Int. J. Remote Sens.* **1996**, *17*, 3001–3014. [CrossRef]

28. Mehrjardi, R.T.; Mahmoodi, S.; Taze, M.; Sahebjalal, E. Accuracy assessment of soil salinity map in Yazd-Ardakan Plain, central Iran, based on Landsat ETM+ imagery. *Am.-Eurasian J. Agric. Environ. Sci.* **2008**, *3*, 708–712.
29. Lillesand, T.M.; Kiefer, R.W. *Remote Sensing and Image Interpretation*; John Wiley & Sons: New York, NY, USA, 2000.
30. Wang, K.L.; Xiong, H.G.; Zang, F. Optimal model of soil pH and influencing factors by using hyperspectral data. *Soils* **2014**, *46*, 544–549.
31. Ong, C.C.H.; Cudahy, T.J. Mapping contaminated soils: Using remotely-sensed hyperspectral data to predict pH. *Eur. J. Soil Sci.* **2014**, *65*, 897–906. [CrossRef]
32. Weng, Y.L.; Gong, P.; Zhu, Z.L. A spectral index for estimating soil salinity in the Yellow River Delta Region of China using EO-1 Hyperion data. *Pedosphere* **2010**, *20*, 378–388. [CrossRef]
33. Liu, H.J.; Zhang, B.; Wang, Z.M.; Song, K.S.; Hu, M.G.; Duan, H.T. Soil saline-alkalization evaluation basing on spectral reflectance characteristics. *J. Infrared Millim. Waves.* **2008**, *27*, 138–142. [CrossRef]
34. Bannari, A.; Guedon, A.M.; El-Harti, A.; Cherkaoui, F.; El-Ghmari, A. Characterization of slightly and moderately saline and sodic soils in irrigated agriculture land using simulated data of advanced land imaging (EO-1) sensor. *Commun. Soil Sci. Plant. Anal.* **2008**, *39*, 2795–2281. [CrossRef]
35. Fan, X.W.; Liu, Y.B.; Tao, J.M.; Weng, Y.L. Soil salinity retrieval from advanced multi-spectral sensor with partial least square regression. *Remote Sens.* **2015**, *7*, 488–511. [CrossRef]
36. Stoner, E.R.; Baumgardner, M.F. *Physiochemical, Site and Bidirectional Reflectance Factor Characteristics of Uniformly Moist Soils*; LARS, Purdue University: West Lafayette, IN, USA, 1980.
37. Metternicht, G.I.; Zinck, J.A. Remote sensing of soil salinity: Potentials and constraints. *Remote Sens. Environ.* **2003**, *85*, 1–20. [CrossRef]
38. McLean, E.O. *Soil pH and Lime Requirement. Methods of Soil Analysis. Part. 2, Chemical and Microbiological Properties*; ASA and SSSA: Madison, WI, USA, 1982.
39. Du, S.; Gao, X.Z. *Technical Specifications of Soil Analysis*, 2nd ed.; Chinese Agricultural Press: Beijing, China, 2006.
40. Morfitt, R.; Barsi, J.; Levy, R.; Markham, B.; Micijevic, E.; Ong, L.; Scaramuzza, P.; Vanderwerff, K. Landsat-8 Operational Land Imager (OLI) radiometric performance on-orbit. *Remote Sens.* **2015**, *7*, 2208–2237. [CrossRef]
41. The United States Geological Survey (USGS). Available online: http://glovis.usgs.gov/ (accessed on 4 May 2015).
42. Adler-Golden, S.M.; Matthew, M.W.; Bernstein, L.S.; Levine, R.Y.; Berk, A.; Richtsmeier, S.C.; Acharya, P.K.; Anderson, G.P.; Felde, G.; Gardner, J.; *et al*. Atmospheric correction for shortwave spectral imagery based on MODTRAN4. *Proc. SPIE* **1999**. [CrossRef]
43. Kruse, A.F. Comparison of ATREM, ACORN, and FLAASH atmospheric corrections using low-altitude AVIRIS data of Boulder, Co. In Proceedings of the Summaries of 13th JPL Airborne Geoscience Workshop, Pasadena, CA, USA, 31 March 2004.
44. Yu, L.Y.; Cai, H.J.; Yao, F.Q.; Zheng, Z.; Wang, J.; Li, Z.J. Applicability of vegetation indices to estimate fractional vegetation coverage. *Trans. Chin. Soc. Agric. Mach.* **2015**, *46*, 231–239.
45. Xu, J.H. *Mathematical Methods in Contemporary Geography*; Higher Education Press: Beijing, China, 2012.
46. Kutner, M.H.; Nachtsheim, C.J.; Neter, J. *Applied Linear Statistical Models*; Irwin: Chicago, IL, USA, 2005.
47. Belsley, D.A.; Kuh, E.; Welsch, R.E. *Regression Diagnostics: Identifying Influential Data and Sources of Collinearity*; John Wiley & Sons: New York, NY, USA, 2005.
48. Chorom, M.; Rengasamy, P. Carbonate chemistry, pH, and physical properties of an alkaline sodic soil as affected by various amendments. *Aust. J. Soil Res.* **1997**, *35*, 149–161. [CrossRef]
49. Chorom, M.; Rengasamy, P.; Murray, R.S. Clay dispersion as infuenced by pH and net particle charge of sodic soils. *Soil Res.* **1994**, *32*, 1243–1252. [CrossRef]
50. López-Granados, F.; Jurado-Expósito, M.; Peña-Barragán, J.M.; García-Torres, L. Using geoestatistical and remote sensing approaches for mapping soil properties. *Eur. J. Agron.* **2005**, *23*, 279–289. [CrossRef]
51. Stoner, F.R. Physicochemical, Site, and Bidirectional Reflectance Factor Characteristics of Uniformly Moist Soils. Ph.D. Thesis, Purdue University, West Lafayette, IN, USA, 1979.
52. Bear, F.E. *Chemistry of the Soil*, 2nd ed.; Reinhold Publication Corporation: New York, NY, USA, 1965.

53. Panda, B.C. *Remote Sensing: Principle and Application*; Viva Books Pvt Ltd.: New Delhi, India, 2005.
54. Farifteh, J.; Farshad, A. Remote sensing and modeling of topsoil properties: A clue for assessing land degradation. In Proceedings of the 17th World Congress of Soil Science CD-ROM Conference, Bangkok, Thailand, 14–21 August 2002.